Proceedings of the ASME 2022
Fluids Engineering Division Summer Meeting
FEDSM2022
August 3-5, 2022, Toronto, Ontario, Canada

FEDSM2022-87577

EFFECT OF ACTIVELY-CONTROLLED TRAILING EDGE FLAP UPON AIRFOIL ENERGY HARVESTER

Jordan Strahl, James Liburdy
Oregon State University
Corvallis, Oregon

ABSTRACT

An experimental study was undertaken to evaluate the power extraction of an airfoil undergoing large amplitude pitching and heaving using a trailing edge flapping motion for the application of energy harvesting for steady flow over the airfoil. The airfoil was a NACA0015 design, pitching at the 1/3 chord position, with an actively controlled trailing edge flap hinged at the 2/3 chord location (chord length of c = 150mm and aspect ratio AR = 2, however end plates were used to simulate a two-dimensional airfoil). Data were obtained over a range of wind speeds corresponding to Reynolds numbers in the 30,000-60,000 range in a low-speed wind tunnel with turbulence intensities below 2%. The results are characterized using the reduced frequency, $k = fc/U_\infty$ over the range of 0.04 - 0.08, where f is the oscillating frequency in Hz, and U_∞ is the freestream velocity. The pitching and heaving amplitudes are $\theta_0 = 70°$ and $h_0 = 0.6c$ respectively, with a phase delay of 90°. Two trailing edge motion profiles are presented, examining the relative phase of trailing edge flap to the pitching phase. For each motion, a positive and negative case are considered. This is a total of 4 trailing edge motion profiles. Trailing edge motion amplitudes of 20° and 40° are compared and results contrasted. Direct transient force measurements were used to obtain the cycle variation of induced aerodynamic loads (lift coefficient) as well as the power output and efficiency. Results are used to identify the influence of trailing edge flap oscillations on the overall performance for energy harvesting, with a maximum efficiency increase of 21.3% and corresponding cycle averaged heaving power coefficient increase of 29.9% observed as a result of trailing edge motion.

NOMENCLATURE

b	foil span
c	foil chord length
C_L	instantaneous coefficient of lift
C_P	instantaneous coefficient of heaving power
$\bar{C}_P$	cycle averaged heaving power coefficient
d	length of foil motion normal to freestream
f	frequency of kinetic motion
F_L	instantaneous lift force
h	instantaneous heaving position
h_0	heaving amplitude
$\dot{h}$	instantaneous heaving velocity
k	reduced frequency
M	instantaneous moment acting upon airfoil
P	instantaneous power extracted
P_s	power supplied by motion of fluid medium
$\bar{P}$	cycle averaged power extraction
t	time
T	period of kinetic motion
U_∞	freestream velocity
θ	instantaneous pitching angle
θ_0	pitching amplitude
$\dot{\theta}$	instantaneous pitching velocity
ρ	freestream fluid density
ϕ	pitching and heaving phase delay

1. INTRODUCTION

Modern society is heavily dependent upon electric power. Maintaining and improving the living standards of a growing population in conjunction with technological surges causes increased energy requirements. This often comes at the expense of increased reliance upon energy sources with adverse environmental impacts, such as the combustion of carbon-based fuels such as coal and gas. The result is emission of carbon dioxide and corresponding adverse environmental effects.

Mitigation of these impacts is highly attractive, but dependent upon a migration to carbon neutral electricity production. While well-known power sources include wind farms, which are known to induce adverse environmental impacts [1], other methods of collecting useful energy in an

environmentally-responsible manner are possible. These methods include airfoil energy harvesters.

Airfoil energy harvesters operate in a bio-inspired periodic motion in order to reduce the velocity of a flow medium and convert fluid kinetic energy to useful electricity. This approach has been shown to be highly efficient, with basic designs obtaining operation efficiencies between 20% and 34% [2-6]. However, the inclusion of more complex geometries, such as the use of flexible wings, attachment of sprung tails, and inclusion of deformable leading and trailing edges, has been shown to improve performance [7-17].

An extensive amount of research has been conducted regarding the usefulness of a modified leading edge, such as actively or passively controlled motion relative to the main foil body [7-11]. Totpal et al. [9] examined a foil with a sprung leading edge which actuated in response to foil inertial forces. Siala et al. [7] performed further experimentation to characterize performance, with results demonstrating that an increase in efficiency of up to 16.7% is possible via implementation of a flexible leading edge. Further experimental research has investigated the impact of varied leading-edge geometries [10] and characterized the performance of actively-controlled leading edge components [8]. In the latter, Prier et al. [8] investigated various leading edge motion profiles using both numerical and experimental methodologies and determined that the proper choice of motion parameters could have a drastic impact upon energy harvesting characteristics, with measured efficiency increases up to 25% relative to rigid foils experiencing the same conditions. Numerical studies have also been conducted to further understand leading edge mechanisms. Tian et al. [3] numerically modeled a rigid plate with flexible leading segment and obtained a 1% increase in power coefficient over a rigid plate. More impressively, when the same configuration was used, but active control for the leading edge implemented, an increase of 11.3% was observed [3].

While trailing edge mechanisms present potential for further device improvement, their performance is not as well understood for energy harvesting purposes. Liu et al. [11] explored the performance of bio-inspired flexible leading and trailing edges, as well as an integrated model utilizing both. In the study, foils were explored both as sole energy extractors and in a parallel twin wing configuration. Their proposed integrated model achieved a 7.68% enhancement over a rigid wing [11]. Further numerical studies have been undertaken to better understand the advantages of sprung and flexible connected tails [11-15] and the advantages of Gurney flaps [16]. Results for sprung tails, which are most similar to the systems considered for the leading edge, show an increase in energy extraction efficiency of 7.24% when compared with a rigid foil [13, 15]. With respect to experimental methods, trailing edge flap vortex dynamics have been investigated [17] and the energy harvesting performance of sprung trailing edges characterized [7]. The latter results are promising, with a measured maximum efficiency increase due to the presence of a sprung trailing edge of 25% over a comparable rigid airfoil [7]. These results seem to indicate that a sprung trailing edge may be advantageous over a sprung connected tail [7, 13, 15].

However, while existing results are both impressive and promising, they are limited. The energy harvesting performance of a foil with an actively controlled trailing edge component is not characterized, and experimental results regarding foils with trailing edge improvements undergoing a kinetic energy extraction regime are largely unavailable. Furthermore, current results indicate that approaches utilizing actively-controlled components or trailing edge modifications offer substantial improvements to device efficiency (25%) relative to other test cases [7, 8, 13, 15]. This makes actively-controlled trailing edge flaps an attractive research area and of experimental interest.

The work presented here serves to further define the energy harvesting performance of an airfoil with an actively-controlled trailing edge undergoing a pitching and heaving regime for the purposes of energy harvesting. Previous research has helped quantify the effect of passive trailing edge motion. However, the novel use of active motion introduces the ability to control and further understand the vortex shedding phenomena that occurs during the pitching and heaving cycle. Optimization of trailing edge motion relative to other kinematic motions by means of a supplied waveform offers the potential to further exploit the favorable pressure gradient experienced by the foil as a consequence of this phenomena, improving lift forces and kinetic energy harvesting. In doing so, four trailing edge motions are considered as well as two trailing edge angular displacement amplitudes.

2. KINEMATIC MOTION

In a kinetic energy harvesting regime, the foil undergoes a periodic flapping motion. The cyclic movement induces an unsteady flow field and periodic vortex shedding occurs. As a consequence, a pressure field which is favorable to the airfoil is induced, resulting in greater lift forces. To achieve this result, sinusoidal pitching and heaving motions are undertaken. A phase shift is introduced, where the pitching motion leads the heaving motion. Mathematically, the motion is described by:

$$h = \mathrm{h}_0 \cos(2\pi f t) \tag{1}$$

$$\theta = \theta_0 \cos(2\pi f t + \phi) \tag{2}$$

where h_0 denotes the heaving amplitude, θ_0 is the pitching amplitude, f is the applied frequency of oscillation, and ϕ is the phase delay between the two motions. In the present study, a phase delay of 90° is employed in conjunction with an applied frequency of oscillation of 1.6 Hz. The pitching amplitude was θ_0 = 70° and the heaving amplitude was h_0 = 0.6c, where c denotes the chord length of the airfoil. Foils possessing these performance characteristics have been shown to harvest flow kinetic energy efficiently [4, 18].

The foil used was a NACA0015 airfoil, which performs well in an energy harvesting regime [18, 20]. The chord length was 150mm and the aspect ratio, the ratio of the foil span to chord

length, was 2. It has been shown that below an aspect ratio of 4, 3-dimensional effects dominate [20]. Therefore, endplates were used to simulate a 2-dimensional system. The pitching axis was located at the one-third chord. This parameter has also been shown to enhance energy harvesting efficiency [18, 21, 22].

Trailing edge motion was accomplished using a motor integrated into the wing design. The motor is situated a distance of 2c/3 from the leading edge and actuates the trailing edge flap, defined as the section of the foil between the trailing edge motor and the trailing edge. A cammed hinge design is employed at the interface to minimize flow through the wing. Figure 1 shows the design CAD model. Figure 2 illustrates the hinge design.

FIGURE 1: SolidWorks CAD model of airfoil design.

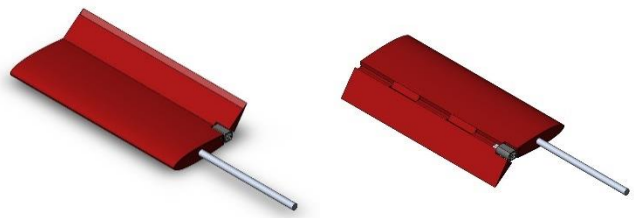

FIGURE 2: Front and back of airfoil at maximum trailing edge deflection angle of 45°.

The integrated trailing edge motor used in the airfoil is a small brushed motor powered by direct current. The motor is fitted with a magnetic encoder which reports the motor shaft position with a precision of ±0.2°. A program authored in LabVIEW 2013 interfaces with the motor and supplies a trapezoidal waveform with variable amplitude and phase. This waveform is periodic and occurs over the same period as the applied pitching and heaving motions. Figure 3 visualizes the supplied signal for each waveform when the amplitude is held at 40° for all trailing edge motions in the first portion of the study. The waveform amplitude is later reduced to 20° for several test cases. The reduced amplitude waveforms are shown in Figure 4. It is worth noting that there is variation in the maximum deflection angle due to friction in the trailing edge motor and gearbox, as well as the necessary presence of small gaps in individual components required for foil assembly.

The two trailing edge phases to be investigated are Phase 1 (P1) and Phase 2 (P2). For each case, a positive and negative motion is identified. This is a total of 4 trailing edge motion profiles. When positive motions are applied, trailing edge deflection is the angular direction opposing the pitching sign during actuation. Negative motions use the same phase as their corresponding positive counterparts, but opposite direction. Of course, during a given motion, the trailing edge is not always oriented in the same direction as the pitching motion. Motor actuation, while in the same direction as pitching sign for positive motions and the opposing direction for negative motions, is not constant due to the nature of the applied trapezoidal wave. Rather, the orientation of the trailing edge is a function both of the sign of the motion and the applied phase relative to pitching and heaving. Figure 5 illustrates the nature of positive and negative motor deflections.

When the trailing edge has reached maximum deflection and is no longer in motion, the foil profile is effectively cambered for a portion of the cycle. Under static conditions, usage of cambered airfoils typically corresponds to greater lift forces. Thereby, it is hypothesized that greater lift force extraction can be obtained by selecting and applying proper deflection techniques.

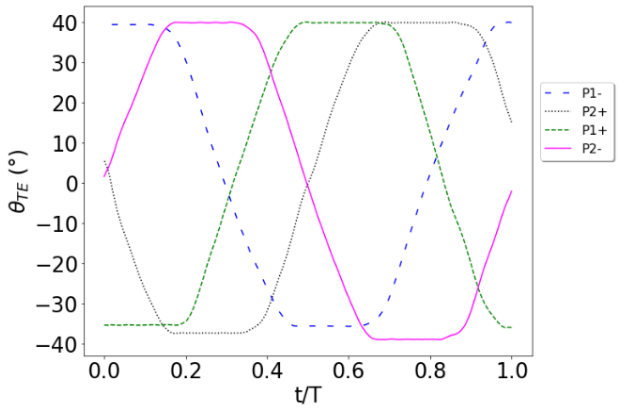

FIGURE 3: Positive and negative cases of both trailing edge motions. Positive and negative cases of Phase 1 (P1) and Phase 2 (P2) are shown.

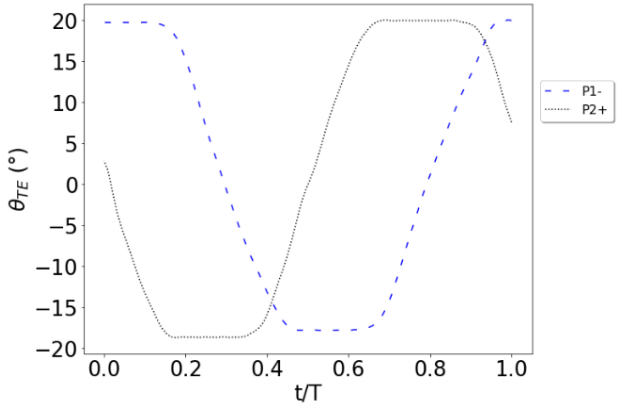

FIGURE 4: Trailing edge motion waveforms with performance characteristics that merit further discussion. The amplitude has been reduced from 40° to 20° for further investigation.

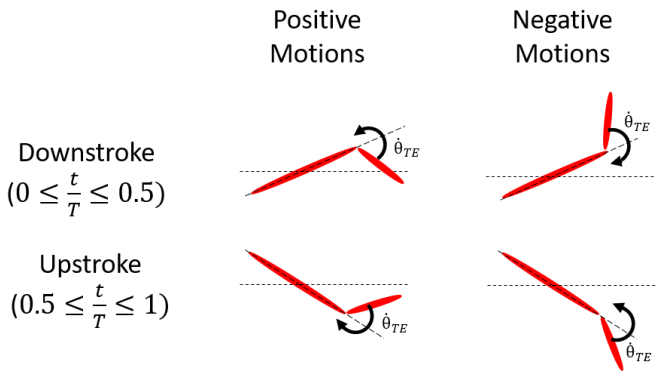

FIGURE 5: Illustration of positive and negative motions. Positive motions actuate the trailing edge in the opposite direction as the sign of the pitching movement, while negative motions act in the same direction as the sign of the pitching movement.

The relationship between the oscillatory timescale and convective timescale further describes motion parameters. This is represented by the reduced frequency, given as:

$$k = \frac{fc}{U_\infty} \tag{3}$$

where c is the foil chord length, U_∞ is the freestream velocity, and f is the frequency of foil oscillation. In the present study, the reduced frequency range is $0.04 \leq k \leq 0.08$. The freestream velocity is varied from $3\text{m/s} \leq U_\infty \leq 6$ m/s, giving a Reynolds number range of 30,000-60,000. Selection of the freestream velocity directly pertains to the magnitude of lift forces exerted on the airfoil. The corresponding coefficient of lift, a key parameter in characterizing the performance of a given test case, is then computed as:

$$C_L = \frac{F_L}{\frac{1}{2}\rho U_\infty^2 cs} \tag{4}$$

where F_L is the measured force normal to the foil body (the measured lift force), ρ is the density of the freestream fluid, c is the foil chord length, and b is the foil span. The instantaneous power extraction of the device is given according to Equation 5:

$$P(t) = F_L(t)\dot{h}(t) + M(t)\dot{\theta}(t) \tag{5}$$

In Equation 5, $\dot{h}(t)$denotes the heaving velocity and $\dot{\theta}(t)$is the pitching velocity. These are the time derivatives of Equation 1 and Equation 2, respectively. The fourth function, M(t), is the moment. However, in the low reduced frequency regime, pitching represents only a small power contribution and only the heave component is considered when evaluating power [2]. Once the power throughout the cycle is known, the cycle averaged power extraction can be computed according to:

$$\bar{P} = \frac{1}{T}\int_t^{t+T} P(t)dt \tag{6}$$

where T is the period of the kinetic energy harvesting cycle. The power coefficient is then defined similarly to the coefficient of lift given in Equation 4:

$$C_P = \frac{P(t)}{\frac{1}{2}\rho U_\infty^3 sc} \tag{7}$$

where s is the foil span. The cycle mean power coefficient is a key parameter is comparing the energy extraction capabilities of different device configurations. This value is defined as:

$$\bar{C}_P = \frac{\bar{P}}{\frac{1}{2}\rho U_\infty^3 sc} \tag{8}$$

The final parameter of interest is the cycle efficiency. This is then evaluated as:

$$\eta = \frac{\bar{P}}{P_s} = \frac{\bar{P}}{\frac{1}{2}\rho U_\infty^3 sd} \tag{9}$$

where P_s is the power supplied by kinetic energy of the flowing fluid medium and d is the swept length perpendicular to the flow during kinetic motion. This is influenced by the selection of trailing edge deflection motion profile, since the maximum swept area is a function of the foil tail location near the beginning and midpoint of the cycle.

3. EXPERIMENTAL METHODS

Experiments were conducted in a closed-loop, recirculating wind tunnel with a test section size of 1.37m x 1.52m and turbulence intensities below 2%. Freestream airflow is delivered by motorized rotation of a propellor. Altering the propellor rotation rate allows the wind speed, measured directly using a manometer in conjunction with a Pitot tube situated upstream of the foil, to be adjusted. The airflow over the apparatus is situated on the downstream side of the propellor to maximize flow stability.

The airfoil body used consists of 3D printed acrylonitrile butadiene styrene (ABS) plastic components, which are hollow in order to minimize mass and therefore inertial forces associated with flapping motion. The pitching axis is equipped with a high-strength aluminum rod that is machined and epoxied along the foil span. Foil flapping motion was accomplished via an in-house built pitching and heaving apparatus controlled using National Instruments 2013 and related hardware. This allows interface with device electrical systems, which accomplish pitching and

heaving motions at the desired flapping motion frequency. A combination of a Scotch yoke and rack-and-pinion mechanisms are employed. The foil is situated vertically in order to isolate flapping motion inertial forces from gravitational effects. Figure 6 shows the mechanical apparatus model. The installed airfoil and utilized endplates, which are situated approximately 4mm from the ends of the airfoil to simulate 2D flow, are shown in Figure 7.

Direct force measurements were taken at 200 Hz using Futek LSB200 load cells and an in-house produced signal amplifier. Since the angle of attack is unsteady, force measurements must be along multiple axes in order to fully describe lift forces throughout the cycle. A pair of load cells was thus used and situated in a housing to minimize crosstalk. Force calibrations were performed prior to experiments.

It has been shown that foil inertial forces associated with flapping motion are substantial when the freestream medium is air [23]. Therefore, each test case was first conducted with an applied wind speed of 0 m/s in order to isolate inertial forces. The desired wind speed is then applied, flow boundaries allowed to develop, and measurements taken. In this second period, the measured forces are representative of the sum of inertial and lift forces. Subtracting the measured isolated inertial forces allows the cyclic lift forces to be isolated. For each portion of the experiment, approximately 90 cycles are considered and an average taken.

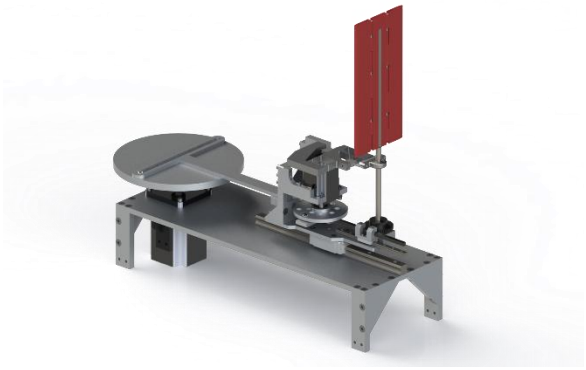

FIGURE 6: In-house manufactured pitching and heaving apparatus used to drive airfoil motion during experiments. Adapted from [23].

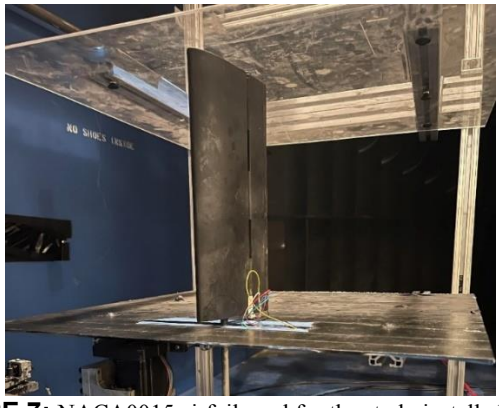

FIGURE 7: NACA0015 airfoil used for the study installed between endplates used to minimize 3D effects.

4. RESULTS AND DISCUSSION

4.1 Effect of Trailing Edge Waveform Phase

The transient coefficient of lift for each waveform shown in Figure 3 and a rigid case taken with the same airfoil are given in Figure 8. The corresponding transient coefficients of heaving power are given in Figure 9, and the calculated efficiencies and cycle mean coefficients of heaving power are given in Figures 10 and 11 respectively. Due to symmetry, only the first half of the cycle is utilized.

The P1- case demonstrates the clearest advantage when compared with the rigid case. It results in a greater maximum lift force at nearly the same time in the cycle ($t/T \approx 0.1$). However, lift forces taper off rapidly from this point. The consequences are a 10.9% reduction in the cycle mean heaving power coefficient compared to the rigid case (see Figure 10 and Figure 11), as well as a further decrease in the efficiency due to a larger swept area for this motion. Further reasons for these results are illustrated well in Figure 8, which reveals that the large lift force peak occurs at in unfortunate time in the cycle while heaving velocity, which is maximized at $t/T = 0.25$, is still relatively small. Further, the secondary peak is relatively small in magnitude and occurs late, resulting in heaving power that reaches an early large peak but is much less substantial throughout the rest of the cycle.

The corresponding positive motion, P1+, manages to delay the maximum lift force until approximately $t/T = 0.22$, significantly closer to the maximum heaving velocity. However, this comes at the expense of a large loss in its magnitude, resulting in a lesser power coefficient. In contrast, the efficiency is only slightly reduced as a consequence of the smaller swept area due to trailing edge deflection at the top of the stroke. Regardless, in terms of power output, P1+ does not perform well.

The P2- test case is the least desirable. It demonstrates the lowest efficiency and cycle mean heaving power coefficient of these cases. The results for maximum lift force are similar to but less pronounced than those of P1+. The maximum lift force is delayed until $t/T \approx 0.15$, but the magnitude is reduced. However, it tapers off remarkably sharply, with the coefficient of lift not exceeding 1 in magnitude anywhere in the $0.25 \leq t/T \leq 0.5$ range. In other words, the secondary peak is suppressed. As illustrated in Figure 9, this comes with a substantial reduction in the area under the coefficient of heaving power curve. This, in conjunction with the reduced magnitude, results in the lowest peak power output and lowest cycle mean coefficient of heaving power measured for all cases for which $k = 0.08$.

In contrast, the P2+ waveform case demonstrates the largest cycle mean heaving power coefficient (an increase of 3.2% over the rigid case), and a greater efficiency than the rigid case (increase of 3.2%). Due to the nature of the motion, the swept area is smaller than that of the P1- motion, further resulting in a greater efficiency. This motion performs well by both delaying the onset of the peak lift force to the latest of all cases and yielding the largest secondary peak of all cases. This delay results in larger lift forces when heaving velocity is close to the maximum value, giving a larger product in Equation 5. The result is a substantial increase in the area under the heaving

power coefficient curve and larger average heaving power output.

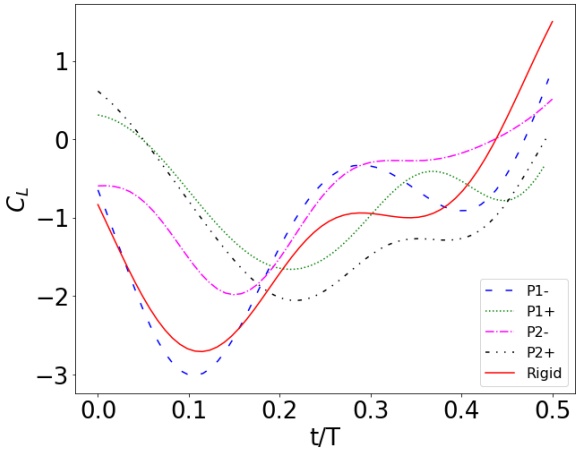

FIGURE 8: Transient coefficients of lift for positive and negative cases of both motion profiles at a trailing edge amplitude of 40° and reduced frequency k = 0.08. Also shown are rigid case results taken with the same airfoil under the same experimental conditions.

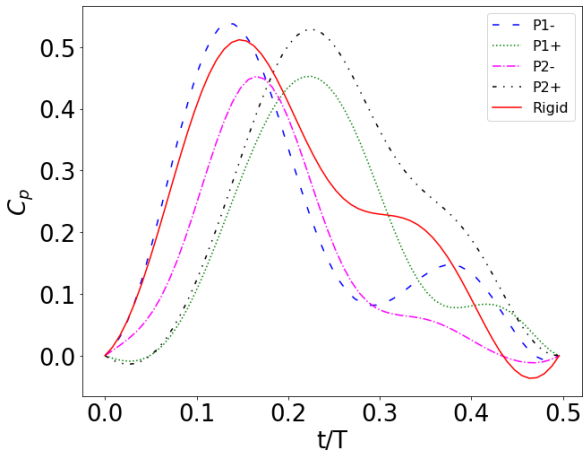

FIGURE 9: Transient coefficients of heaving power for positive and negative cases of both motion profiles at a trailing edge amplitude of 40° and reduced frequency k = 0.08. Also shown are rigid case results taken with the same airfoil under the same experimental conditions.

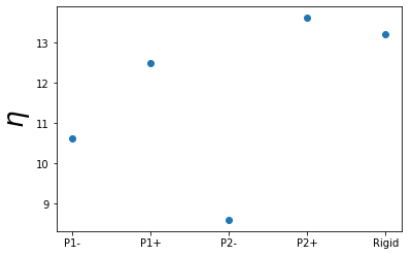

FIGURE 10: Cycle efficiency for positive and negative cases of both motion profiles at a trailing edge amplitude of 40° and reduced frequency k = 0.08 shown with datum rigid case results.

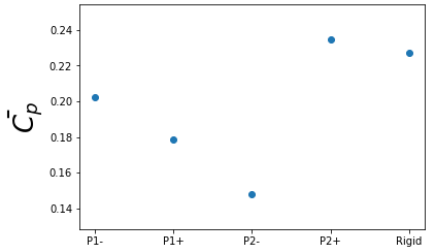

FIGURE 11: Cycle mean heaving power coefficient for positive and negative cases of both motion profiles at a trailing edge amplitude of 40° and reduced frequency k = 0.08 shown with datum rigid case results.

4.2 Effect of Trailing Edge Deflection Angle

When trailing edge amplitudes of 40° were employed, both P1- and P2+ demonstrated promising results at k = 0.08. In response, the trailing edge angular displacement amplitude was adjusted from 40° to 20° and those test cases investigated once more, at the same reduced frequency. Figure 12 shows the transient coefficient of lift for each of these new test cases, along with the previous results for the same motions with the larger trailing edge flap deflection angle and the rigid case. The corresponding transient coefficients of heaving power are shown in Figure 13. Figure 14 shows the cycle efficiency for these two motion profiles and the rigid case at reduced frequencies of 0.08, 0.06, and 0.04. The cycle mean heaving power coefficients corresponding to Figure 14 are given in Figure 15.

When the trailing edge deflection amplitude is reduced for P1-, the result is remarkably favorable. While use of the larger deflection corresponded to an efficiency reduction to below that of the rigid case, the same waveform at the reduced amplitude improves the efficiency, yielding an increase of 2.7% over the rigid case results under the same conditions. While the increase in swept area observed by the larger amplitude case is also in effect, the smaller deflection results in a slightly smaller swept area compared to the larger deflection, but still greater than that of the rigid case. The increase in efficiency is also a consequence of an improvement in the cycle mean heaving power coefficient relative to the rigid case. An increase of 10.0% is observed. This is because the smaller amplitude case delays the onset of peak lift forces to t/T ≈ 0.15 but preserves a portion of the magnitude increase. The secondary lift force peak occurs slightly sooner and with an improvement in magnitude over the higher amplitude case. As illustrated in Figure 13, the result is one of the largest magnitudes of coefficient of heaving power measured as well as a greater power output throughout the later part of the half-cycle.

Reducing the motion amplitude for P2+ also proves to be fruitful. At the reduced amplitude, an increase of 10.7% in both efficiency and cycle averaged heaving power coefficient is observed over the rigid case. At the greater amplitude, efficiency and cycle averaged heaving power coefficient increases of only 3.2% were obtained over rigid case results. In terms of lift forces, the reduced amplitude cycle performs much closer to the P1- case at the lower 20° amplitude. The reduction in peak magnitude becomes an increase, but is not delayed as late in the cycle. However, the magnitude of the increase results in the greatest

maximum lift force measurement shown in Figure 12. When coupled with a delayed onset, this results in the greatest maximum heaving power coefficient in Figure 13. Although lift forces are reduced more sharply before the onset of the second peak, performance is enhanced and the improvement in cycle averaged heaving power coefficient relative to the rigid case is very similar to that of the reduced amplitude P1- case. However, the swept area is greater for P1-, yielding a less desirable efficiency improvement.

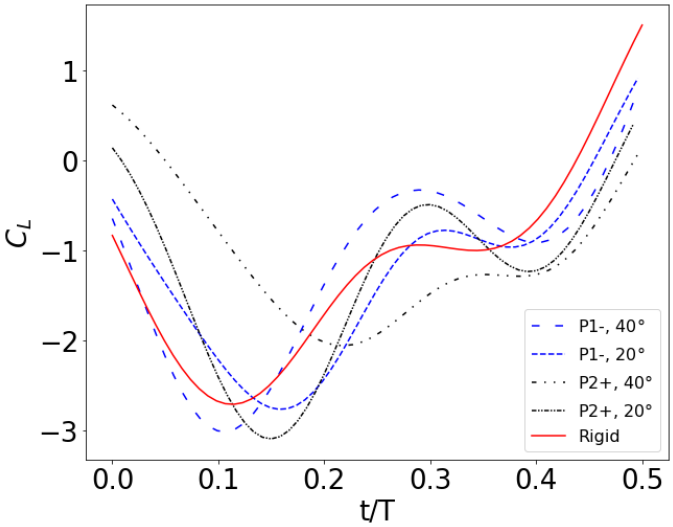

FIGURE 12: Transient coefficients of lift for P1- and P2+ trailing edge motions at trailing edge amplitudes of 40° and 20° with reduced frequency k = 0.08. Also shown are rigid case results taken with the same airfoil under the same experimental conditions.

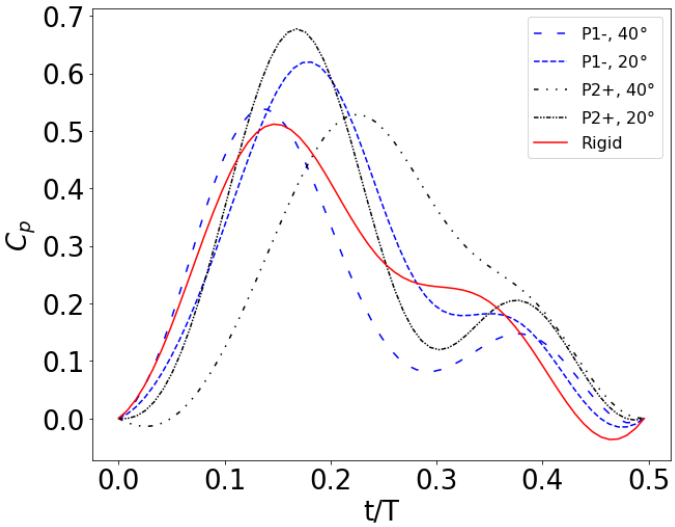

FIGURE 13: Transient coefficients of heaving power for P1- and P2+ trailing edge motions at trailing edge amplitudes of 40° and 20° with reduced frequency k = 0.08. Also shown are rigid case results taken with the same airfoil under the same experimental conditions.

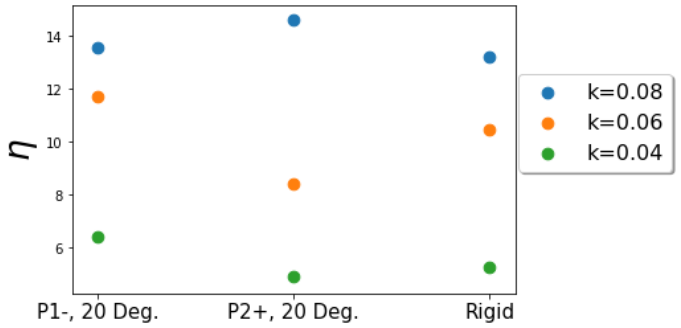

FIGURE 14: Cycle efficiency for the rigid case and the P1- and P2+ trailing edge motion cases at a trailing edge amplitude of 20° and reduced frequencies k = 0.08, 0.06, and 0.04.

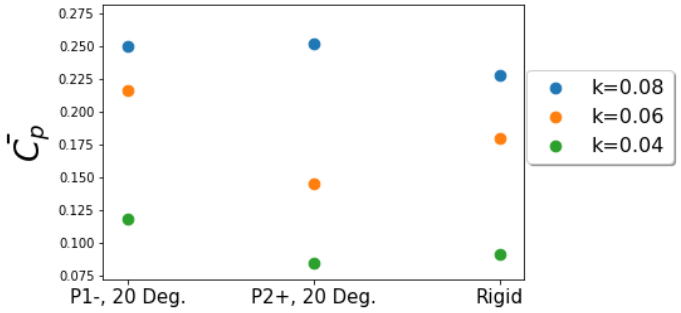

FIGURE 15: Cycle mean heaving power coefficient for the rigid case and the P1- and P2+ trailing edge motion cases at a trailing edge amplitude of 20° and reduced frequencies k = 0.08, 0.06, and 0.04.

4.3 Effect of Reduced Frequency

The final portion of direct force measurements entailed quantifying the effect of reduced frequency upon trailing edge motion performance relative to the rigid case. Two trailing edge motions, P1- and P2+, were again investigated at a trailing edge amplitude of 20°. While all previous experiments were performed only for a reduced frequency of k = 0.08, these two test cases and the rigid one (as a basis for comparison) were performed again at k = 0.06 and k = 0.04. To do so, the wind speed was increased while flapping frequency and foil chord length remained constant. Results for k = 0.06 are given in Figures 14, 15, 16, and 17. Results for k = 0.04 are described by Figures 14, 15, 18, and 19.

The behavior of the P1- test case relative to the rigid one is the same for both lower values of reduced frequency: The secondary lift force peak value is approximately the same and occurs slightly later in the cycle, while the greatest lift force magnitude is larger and significantly delayed. For k = 0.06, the rigid foil experiences a maximum lift force at t/T ≈ 0.19, while the P1- trailing edge motion profile manages to delay this occurrence until t/T ≈ 0.23, very close to the heaving velocity maximum. For k = 0.04, the rigid foil's maximum is at t/T = 0.10 while the P1- motion profile does not reach its maximum until t/T ≈ 0.16. In both cases, the consequence is again a stark increase in the maximum of the coefficient of heaving power, as

well as a larger area under the curve. As a result, both the efficiency and cycle mean power coefficient are improved over the rigid case for each k value. Use of the P1- motion at the reduced trailing edge amplitude of 20° results in top power extraction performance, with an efficiency increase of 12.2% and cycle mean heaving power coefficient increase of 20.1% for k = 0.06. For k = 0.04, these values are 21.3% and 29.9%, respectively.

However, the performance improvement trend observed for P2+ does not continue at these lower values of reduced frequency. At k = 0.06, the utilization of this motion profile not only inhibits the magnitude of the lift force maximum, but causes it to be reached earlier in the cycle, when heaving velocity is at a lower magnitude. While the magnitude of the second peak is improved, the result is not drastic enough to resolve the shortcomings associated with the larger one. Further, it occurs so late in the cycle (when heaving velocity is reduced), that its impact on power efficiency is minimal relative to the effect on the larger peak. As a result, the power extraction of the device is inhibited and the cycle efficiency and mean heaving power coefficient are both reduced relative to the rigid case by a factor of 19.4%. When k = 0.04, results show that maximum lift force is again delayed at the expense of magnitude. However, the observed delay is remarkably small (see Figure 18) and the magnitude reduction relatively large in size. As a consequence, the power coefficient is slightly reduced at its peak. However, a larger expense is paid later on in the cycle, between t/T ≈ 0.25 and 0.38, where lift forces are reduced and the heaving power correspondingly lower for a substantial portion of the cycle. This substantially inhibits both the cycle efficiency and cycle mean power coefficient of the device, which are both reduced by 7.1% relative to the rigid case.

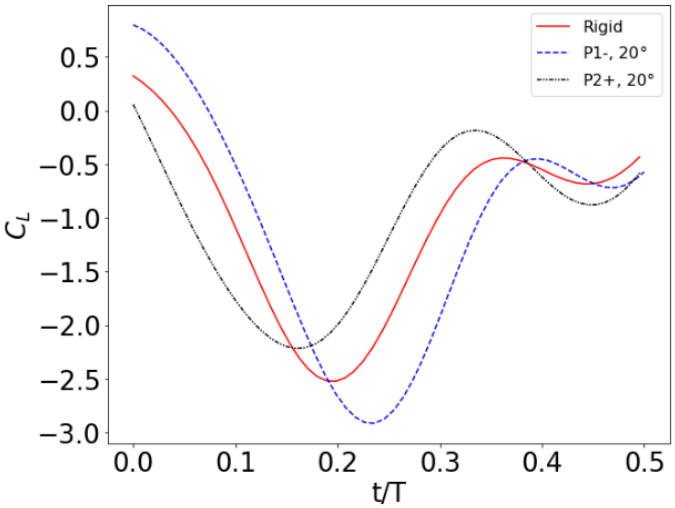

FIGURE 16: Transient coefficients of lift for P1- and P2+ trailing edge motions with a trailing edge amplitude of 20° at reduced frequency k = 0.06. Also shown are rigid case results taken with the same airfoil under the same experimental conditions.

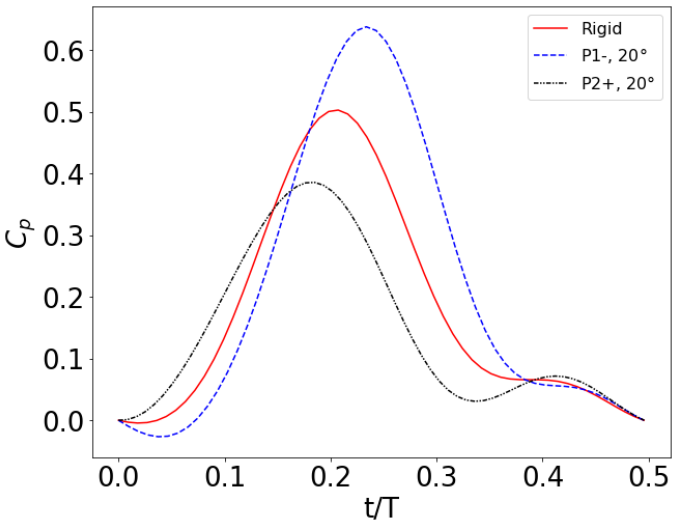

FIGURE 17: Transient coefficients of heaving power for P1- and P2+ trailing edge motions with a trailing edge amplitude of 20° at reduced frequency k = 0.06. Also shown are rigid case results taken with the same airfoil under the same experimental conditions.

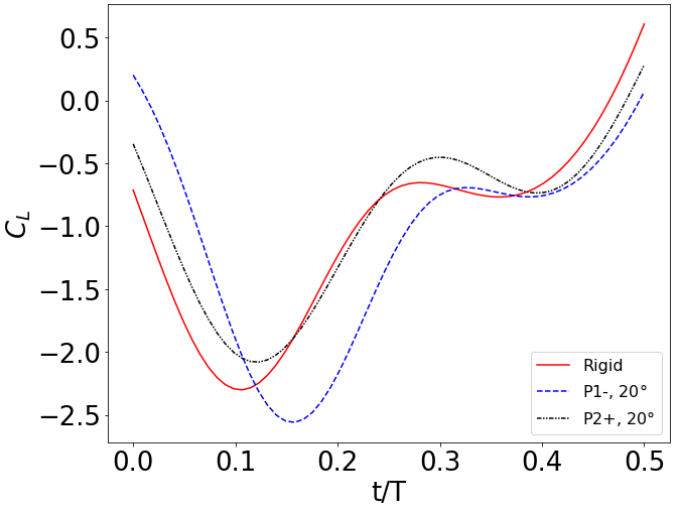

FIGURE 18: Transient coefficients of lift for P1- and P2+ trailing edge motions with a trailing edge amplitude of 20° at reduced frequency k = 0.04. Also shown are rigid case results taken with the same airfoil under the same experimental conditions.

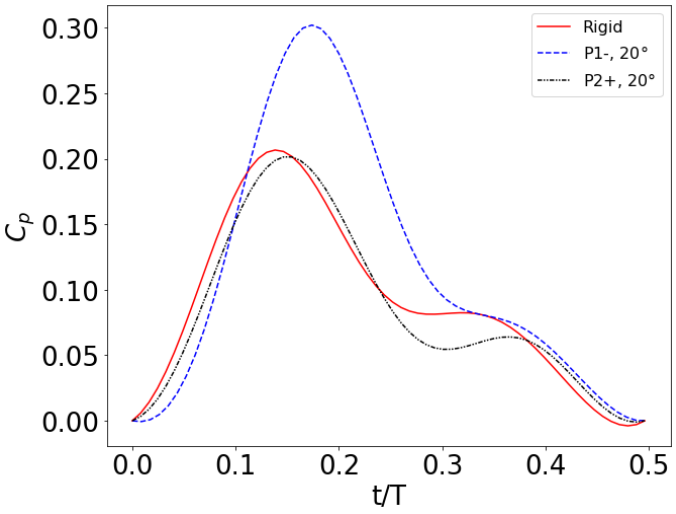

FIGURE 19: Transient coefficients of heaving power for P1- and P2+ trailing edge motions with a trailing edge amplitude of 20° at reduced frequency k = 0.04. Also shown are rigid case results taken with the same airfoil under the same experimental conditions.

5. CONCLUSION

An experimental study entailing direct force measurements was performed to investigate the impact of actively controlled trailing edge motion upon the kinetic energy harvesting capabilities of a NACA0015 airfoil undergoing pitching and heaving. It has been demonstrated that the proper selection of trailing edge motion phase relative to sinusoidal pitching and heaving has a direct influence upon the magnitude and timing of peak lift forces. This, in turn, impacts power output of the device.

Two trailing edge motion phases were investigated, each with a positive case and a negative case for a total of 4 trailing edge motions. Two of these test cases, P1- and P2+, were selected for examination with reduced amplitudes. In both cases, this improved the results substantially. It is concluded that lower amplitude trailing edge motions can offer more significant improvements under the conditions examined. However, the selection of positive and negative motions is a parameter that must be carefully selected in conjunction with other trailing edge motion aspects. While Phase 1 performed best when negative motion was applied, Phase 2 was better suited as a positive motion.

Under static conditions, cambered airfoils experience greater lift forces than their symmetric counterparts. The timing of trailing edge motion actuation influences the camber of the airfoil during critical points in the cycle, including the midpoint of the half-cycle when heaving velocity is maximized. It is thought that the result is an influence upon the timing and strength of shed vortices, resulting in more preferable timing and larger strength of the favorable pressure gradient exploited by the foil during its cycle for energy harvesting. A future flow visualization study is of interest to further investigate this. The test case that demonstrates the greatest improvement over the rigid case on both a basis of efficiency and heaving power coefficient is P1- at a trailing edge angular displacement of 20°. It offers increases of 21.3% and 29.9% respectively at a reduced frequency of k = 0.04 and corresponds to a greater power extraction than rigid case results at all reduced frequencies examined.

ACKNOWLEDGEMENTS

The authors would like to acknowledge the financial support provided by the National Science Foundation Award Number 1804964.

REFERENCES

[1] Everaert, J., "Wind Turbines and Birds in Flanders: Preliminary Study Results and Recommendations," Pennsylvania State University, University Park, Pennsylvania.

[2] Kinsey, T. and Dumas, G., 2008. "Parametric study of an oscillating airfoil in a power-extraction regime". *American Institute of Aeronautics and Astronautics Journal,* ***46***, pp. 1318-1330.

[3] Tian, F.-B., Young, J., and Lai, J. C., 2014. "Improving power-extraction efficiency of a flapping plate: From passive deformation to active control". *Journal of Fluids and Structures,* ***51***, pp. 384-392.

[4] Zhu, Q., 2011. "Optimal frequency for flow energy harvesting of a flapping foil". *Journal of Fluid Mechanics,* ***675***, pp. 495-517.

[5] Jamil, M., and Javed, A., 2019. "Design optimization of a Semi-Active Flapping Foil in an Energy Extraction Mode". *2019 International Conference on Engineering and Emerging Technologies (ICEET)*, pp. 1-8.

[6] Kim, D., Strom, B., Mandre, S., and Breuer, K., 2017. "Energy harvesting performance and flow structure of an oscillating hydrofoil with finite span". *Journal of Fluids and Structures,* ***70***, pp. 314–326.

[7] Siala, F. F., Fard, K. K., and Liburdy, J. A., 2020. "Experimental study of inertia-based passive flexibility of a heaving and pitching airfoil operating in the energy harvesting regime". *Physics of Fluids,* ***32***, p. 017101.

[8] Prier, M. W., and Liburdy, J. A., 2019. "Discrete Vortex Modeling of a Flapping Foil With Activated Leading Edge Motion." *Proceedings of the ASME-JSME-KSME 2019 8th Joint Fluids Engineering Conference. Volume 1: Fluid Mechanics. San Francisco, California, USA. July 28–August 1, 2019. V001T01A086. ASME.*

[9] Totpal, A. D., Siala, F. F., and Liburdy, J. A., 2018. "Energy harvesting of an oscillating foil at low reduced frequencies with rigid and passively deforming leading edge". *Journal of Fluids and Structures,* ***82***, pp. 329–342.

[10] Rival, D., Kriegseis, J., Schaub, P., Widmann, A., and Tropea, C., 2014. "Characteristic length scales for vortex detachment on plunging profiles with varying leading-edge geometry". *Experimental Fluids,* ***55***, p. 1660.

[11] Liu, W., Xiao, Q., and Cheng, F., 2013. "A bio-inspired study on tidal energy extraction with flexible flapping

wings". *Bioinspiration Biomimetics,* ***8***(3).
[12] Wu, J., Shu, C., Zhao, N., and Tian, F.-B., 2015. "Numerical study on the power extraction performance of a flapping foil with a flexible tail". *Physics of Fluids,* ***27***, 01, p. 013602.
[13] Liu, W., Xiao, Q., and Zhu, Q., 2016. "Passive flexibility effect on oscillating foil energy harvester". *AIAA Journal,* ***54***(1), pp. 1172–1187.
[14] Wu, J., Wu, J., Tian, F.-B., Zhao, N., and Li, Y.-D., 2015. "How a flexible tail improves the power extraction efficiency of a semi-activated flapping foil system: A numerical study". *Journal of Fluids and Structures,* ***54***, pp. 886-899.
[15] Liu, Z., Tian, F.-B., Young, J., and Lai, J., 2017. "Flapping foil power generator performance enhanced with a spring-connected tail". *Physics of Fluids,* ***29***, 12.
[16] Zhu, B., Huang, Y., and Zhang, Y., 2018. "Energy harvesting properties of a flapping wing with a adaptive gurney flap". *Energy,* ***152***, 06, pp. 117–128.
[17] Mancini, P., Medina, A., and Jones, A.m 2019. "Experimental and analytical investigation into lift prediction on large trailing edge flaps". *Physics of Fluids,* ***31***, p. 013106.
[18] Kinsey, T., and Dumas, G., 2006, "Parametric Study of an Oscillating Airfoil in Power Extraction Regime," *24th Applied Aerodynamics Conference*, 2006.
[19] Deng, J., Caulfield, C. P., and Shao, X., 2014. "Effect of aspect ratio on the energy extraction efficiency of three-dimensional flapping foils". *Physics of Fluids,* ***26***(4).
[20] Lindsey, K., 2002. "A Feasibility Study of Oscillating-Wing Power Generators". Master's thesis, Naval Postgraduate School, Monterey, California.
[21] Liu, Z., Bhattacharjee, K. S., Tian, F.-B., Young, J., Ray, T., and Lai, J. C. S., 2019. "Kinematic optimization of a flapping foil power generator using a multi-fidelity evolutionary algorithm". *Renewable Energy,* ***132***, pp. 543-557.
[22] Duarte, L., Dellinger, N., Dellinger, G., and Ghenaim, A., 2021. "Experimental optimization of the pitching structural parameters of a fully passive flapping foil turbine". *Renewable Energy,* ***171***, pp. 1436-1444.
[23] Totpal, A., 2017. "The Energy Extraction Performance of an Oscillating Rigid and Flexible Foil". Master's thesis, Oregon State University, Corvallis, Oregon.

